ACS NANO
Cite This: ACS Nano XXXX, XXX, XXX−XXX
www.acsnano.org
ARTICLE

Highly Sensitive Bulk Silicon Chemical Sensors with Sub-5 nm Thin Charge Inversion Layers

Hossain M. Fahad,[†,‡,§,⊥] Niharika Gupta,[†,⊥] Rui Han,[†] Sujay B. Desai,[†,‡,§] and Ali Javey*[,†,‡,§]

[†]Electrical Engineering & Computer Sciences, University of California, Berkeley, California 94720, United States
[‡]Berkeley Sensor and Actuator Center, University of California, Berkeley, California 94720, United States
[§]Materials Sciences Division, Lawrence Berkeley National Laboratory, Berkeley, California 94720, United States

Supporting Information

ABSTRACT: **There is an increasing demand for mass-producible, low-power gas sensors in a wide variety of industrial and consumer applications. Here, we report chemical-sensitive field-effect-transistors (CS-FETs) based on bulk silicon wafers, wherein an electrostatically confined sub-5 nm thin charge inversion layer is modulated by chemical exposure to achieve a high-sensitivity gas-sensing platform. Using hydrogen sensing as a "litmus" test, we demonstrate large sensor responses (>1000%) to 0.5% H_2 gas, with fast response (<60 s) and recovery times (<120 s) at room temperature and low power (<50 μW). On the basis of these performance metrics as well as standardized benchmarking, we show that bulk silicon CS-FETs offer similar or better sensing performance compared to emerging nanostructures semiconductors while providing a highly scalable and manufacturable platform.**

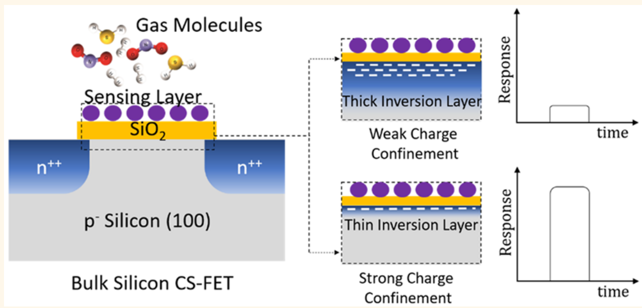

KEYWORDS: *CS-FET, electrostatic confinement, CMOS gas sensors, tunable sensitivity, low power, charge inversion layer*

In recent years, the micro-hotplate-based resistive ceramic sensor has been the dominant commercial technology for miniaturized gas-sensing applications. These sensors are made of thick (hundreds of nanometers) films of transition metal oxides, for example ZnO, SnO_x, and InO_x, that get oxidized or reduced by a target gas at high temperatures.[1,2] Consequently, this technology suffers from high power consumption requirements (≫1 mW). Furthermore, such ceramic films need to be electrically conductive, thereby limiting the choice of metal oxides that can be used for sensing and contributing to poor selectivity against interfering gases. Despite these drawbacks, major manufacturers continue to develop portable gas sensors based on this technology. Resistive sensors based on metallic nanowires (Pd, Pt) have also shown promise for low-power hydrogen gas sensing.[3,4] However, their applicability to detect other gases remains mostly undetermined.

Another promising class of sensors is based on functionalized field-effect transistors (FETs).[5−9] Chemical-sensitive FET (CS-FET) sensors based on low-dimensional nanomaterials such as carbon nanotubes, silicon nanowires, graphene, and transition metal dichalcogenides have shown high sensitivity in detecting a wide variety of gases at room temperature.[10−24] This is primarily due to (i) a large surface area to volume ratio and (ii) confinement of charge transport in one or two dimensions. Among these materials, pristine single-crystalline silicon is comparatively inert and can respond to specific gases only upon functionalization with appropriate chemical-sensitive layers. We recently demonstrated this selectivity advantage using ultra-thin-body (3.5 nm) silicon CS-FETs integrated with different chemical-sensing layers (∼5 nm thin metal alloys) sensitive to specific gases.[25] While such nanoscale silicon can provide high sensitivity, thickness uniformity control across wafers can lead to process, cost, and yield complexities in large-scale manufacturing. On the other hand, conventional bulk silicon transistors do not have a physically thin channel, resulting in less susceptibility to such complexities, and can be manufactured very economically.

In this work, we demonstrate bulk silicon CS-FETs as a highly sensitive low-power gas-sensing platform. The well-established concept of few nanometers thin inversion layers in conventional MOSFETs is adopted here using proper device architecture and operating voltage conditions. Through the electrostatic confinement of the inversion layer, the capacitive coupling between the sensing layer and channel is maximized, enabling high detection sensitivity. To evaluate this platform, hydrogen gas sensing is used as the test application. Monitoring hydrogen leaks is becoming increasingly important in several

Received: January 23, 2018
Accepted: February 17, 2018
Published: February 17, 2018

DOI: 10.1021/acsnano.8b00580
ACS Nano XXXX, XXX, XXX−XXX

applications, requiring stable sensors that can detect below the lower explosion limit of 4% (v/v in air) at low power, low cost and with a very small form factor.[26]

DEVICE DESCRIPTION

Conceptually, bulk silicon CS-FETs are similar to conventional enhancement-mode silicon transistors with the exception of the electrically active gate stack that is replaced by a large surface area, ultrathin chemical sensing layer, as depicted in Figure 1.

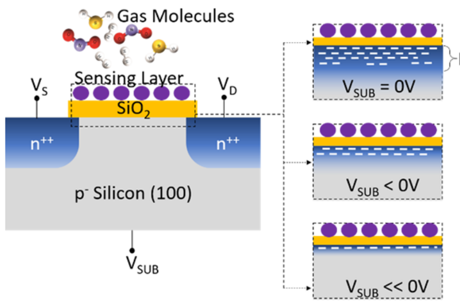

Figure 1. Cross-sectional schematic of a bulk silicon CS-FET with electrostatic confinement of the charge inversion layer for achieving high sensitivity.

This sensing layer is electrically floating and can be engineered to be sensitive to a target gas, where interactions can lead to reversible changes in work function and/or morphology. For the purpose of this work, ultrathin sensing layers composed of Ni (0.3 nm) and Pd (1 nm) are used for H_2 gas sensing, where H_2 readily dissociates over Pd at room temperature into atomic hydrogen, leading to the formation of PdH_x.[27] CS-FETs are configured as n-type transistors with light p-body doping (~8 × 10^{14} boron atoms cm^{-3}), and the electrically floating sensing layer is capacitively coupled to the silicon channel *via* the native oxide (effective oxide thickness, EOT, of 2.5 to 3 nm). The sensitivities of these sensors are dependent on the threshold voltage of the transistors.

Under equilibrium and ambient conditions, the CS-FET threshold voltage (V_t) is determined by the body doping and the effective work function (EWF) of the sensing layer, which for ultrathin Ni–Pd is expected to be lower (~4.2 eV) than bulk values (~5.11 eV) due to work-function dependence on metal thickness.[28] If the V_t is sufficiently low, an inversion layer of electrons (transistor channel) is created at the Si/SiO_2 interface. The total electron density and thickness of the inversion layer (which is directly dependent on V_t) can then be controlled by applying a reverse bias to the silicon substrate (also called body), as depicted in Figure 1. In conventional transistors, this mechanism of V_t control is called the "body effect", where an appropriate body voltage (V_{SUB}) effectively controls the p–n junction formed between the p-body and the n-inversion-layer. From a sensors perspective, this provides a highly tunable operation for CS-FETs, where the device can be tuned to the optimal performance by using V_{SUB}. Equation 1 describes the relation between applied body bias and threshold voltage:

$$\Delta V_t = \frac{\sqrt{2\varepsilon_s q N_{SUB}}}{C_{ox}}[(2\varphi_F + (V_s - V_{SUB}))^{1/2} - (2\varphi_F)^{1/2}] \quad (1)$$

where ε_s is the dielectric permittivity of silicon, q is the electron charge, N_{SUB} is the body doping, C_{ox} is the capacitance of the native oxide, V_s is the source voltage (ground), φ_F is the potential difference between the mid-gap and Fermi energy levels of the silicon body and V_{SUB} is the applied body bias.[29]

RESULTS AND DISCUSSION

Device Modeling and Simulation. A physical understanding of the sensing mechanism in bulk silicon CS-FET gas sensors is presented in Figure 2 using TCAD (Synopsys v.2016) device modeling and simulations. Table 1 lists the parameters used in simulating the n-type transistors where the sensing layer work function is set at 4.2 eV. Details on device modeling and simulation are in the Methods section.

Table 1. CS-FET Device Parameters

parameter	value
gate length (L_g)	3 μm
effective oxide thickness (EOT)	3 nm
source/drain doping	1 × 10^{20} cm^{-3}, phosphorus
body doping (N_{SUB})	8 × 10^{14} cm^{-3}, boron

As it can be seen in Figure 2a, at V_{SUB} = 0 V, a simulated peak electron density of 2 × 10^{16} cm^{-3} is observed at an inversion layer depth of 3.3 nm with a total inversion layer thickness (T_{inv}) of 17.4 nm. T_{inv} is extracted as the location of the charge centroid in Figure 2a, and the electron density distribution is extracted across the midpoint of the CS-FET silicon channel. Applying V_{SUB} = −4 V lowers the peak electron density to 0.65 × 10^{16} cm^{-3} at an inversion layer depth of 2.7 nm and a T_{inv} of 6.3 nm. With higher reverse body bias, the inversion layer is not only thinner but also pushed closer to the interface of the native

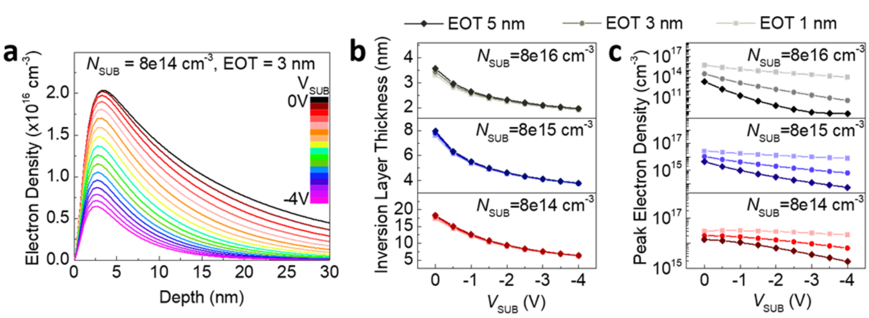

Figure 2. Characteristic of simulated silicon CS-FET devices depicting (a) inversion layer profiles, (b) extracted inversion layer thickness (sensing layer work function (Φ_m) is set to 4.2 eV), and (c) peak electron density at different body biases. (Note: Inversion layer profiles are extracted across the channel midpoint of the simulated device.)

DOI: 10.1021/acsnano.8b00580
ACS Nano XXXX, XXX, XXX−XXX

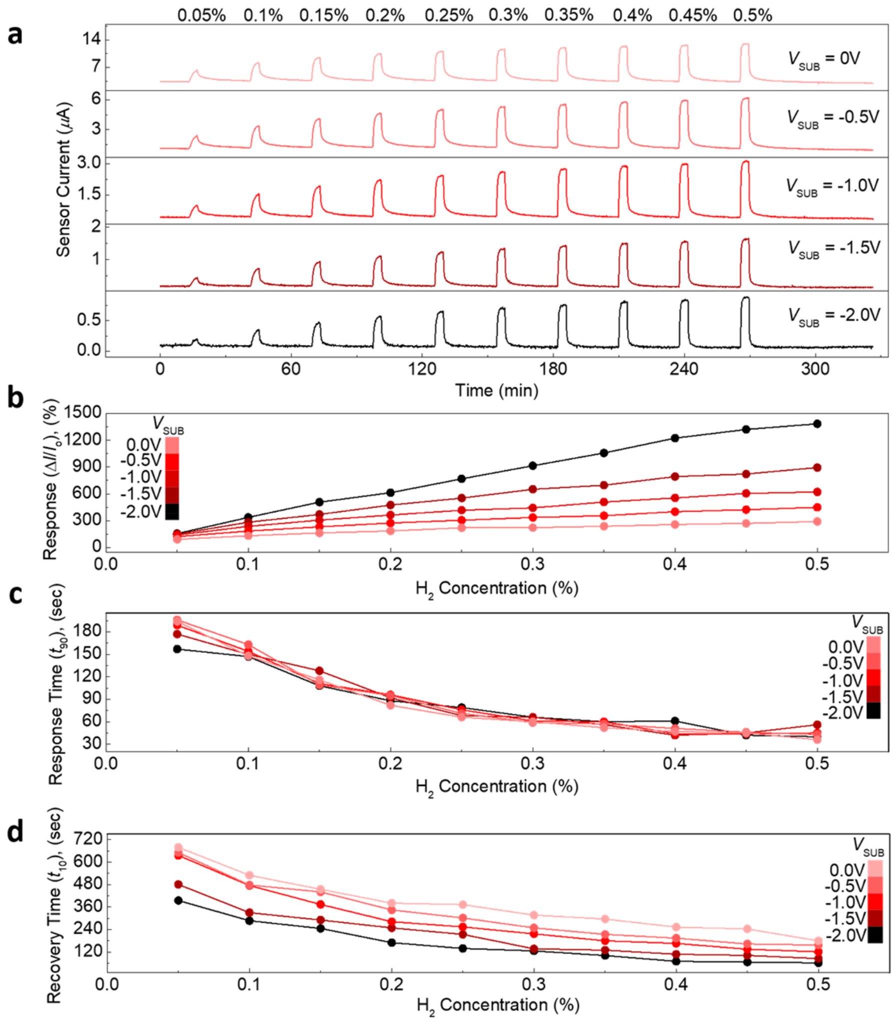

Figure 3. (a) Experimentally measured current of a Ni–Pd CS-FET in response to different H_2 concentrations and at different body biases (V_{DS} = 3 V, RH < 10%). (b) Extracted sensor response ($\Delta I/I_o$) *vs* H_2 concentrations, (c) t_{90} *vs* concentration, and (d) t_{10} *vs* concentration from panel (a) at different V_{SUB}.

oxide and silicon, leading to improved electrostatic control in the channel by the sensing layer. As will be seen in the subsequent sections, this drastically improves sensor response and sensitivity.

Next, we explore various device parameters that can be varied to optimize the charge inversion layer. T_{inv} is inversely dependent on body doping (N_{SUB}), as shown in Figure 2b. As N_{SUB} is increased from 8 × 10^{14} cm^{-3} to 8 × 10^{16} cm^{-3} of boron atoms, T_{inv} (at V_{SUB} = −4 V, EOT = 3 nm) is reduced from 6.3 nm to 2 nm. Body doping and charge density in the inversion layer are also inversely related to each other. As indicated in Figure 2c, increasing N_{SUB} from 8 × 10^{14} cm^{-3} to 8 × 10^{16} cm^{-3} of boron, leads to a decrease in peak electron density ($n_{electron}$) from 0.65 × 10^{16} cm^{-3} to 0.4 × 10^{11} cm^{-3} (V_{SUB} = −4 V, EOT = 3 nm). The effect of oxide thickness on T_{inv} is minimal, as seen in Figure 2b, where only at low V_{SUB} does EOT reduction lead to minimal decrease in T_{inv}. Reducing the EOT from 5 nm to 1 nm leads to an increase in peak electron density from 0.5 × 10^9 cm^{-3} to 1 × 10^{14} cm^{-3} (V_{SUB} = −4 V, N_{SUB} = 8 × 10^{16} cm^{-3}). Based on this discussion, body doping and effective oxide thickness are key optimization parameters to consider in designing a sensitive bulk CS-FET gas sensor. However, it is important to note that T_{inv}, $n_{electron}$, EOT, and N_{SUB} are intricately linked to each other and that the above discussion provides highly generalized guidelines for CS-FET sensor design based on simulation results.

Experimental Validation of Correlation between Sensitivity and Inversion Layer Thickness. Bulk silicon CS-FETs are fabricated using a fully CMOS-compatible, gate-last processing scheme (see Methods section and Supporting Information S1), where the Ni–Pd sensing layer is deposited in the penultimate process step. Following this, the sensor is annealed in N_2 at 150 °C for 1 h. Figure 3a shows the experimentally measured room-temperature sensor response of a Ni–Pd CS-FET to different concentrations of hydrogen ranging from 0.05% to 0.5% (diluted in dry air) in steps of 0.05%, at different body biases. Details on the measurement apparatus can be found in the Methods section. With increasing reverse body bias from 0 V to −2 V, % sensor response ((I_{peak} − $I_{baseline}$)/$I_{baseline}$) to 0.5% H_2 concentration increases from 291% to 1383%, as indicated in Figure 3b. Furthermore, sensor linearity is also drastically improved, where the sensitivity increases from 0.04%/ppm to 0.27%/ppm upon changing body biases from 0 V to −2 V. Here, sensitivity is defined as the slope of the % sensor response ((I_{peak} − $I_{baseline}$)/$I_{baseline}$) per ppm of hydrogen gas. It is to be noted that variations in processing conditions of the sensing layer, for example, annealing in forming gas instead of N_2, can result in high sensor responses

DOI: 10.1021/acsnano.8b00580
ACS Nano XXXX, XXX, XXX−XXX

(~15 000%) (shown in Supporting Information S2). This is due to formation of large-size Pd clusters providing increased surface area for H_2 interaction. However, this negatively impacts sensor response time due to longer H_2 diffusion paths. It is also important to note that bare silicon CS-FETs without any sensing layers do not show any response to hydrogen (see Supporting Information S3). Figure 3c shows the sensor response time (t_{90}) *vs* hydrogen concentration, with minimum and maximum $t_{90} \approx 36$ s (for 0.5% H_2) and 196 s (for 0.05% H_2), respectively. t_{90} is defined as the time taken for the sensor to reach 90% of its peak response value from the baseline current. Varying the body bias appears to have no significant effect on sensor response time. This is expected, as response times are dependent on the rate at which hydrogen diffuses and adsorbs on the Ni–Pd sensing layer.[30] Figure 3d depicts the room-temperature recovery times (t_{10}) for different hydrogen concentrations, with minimum and maximum t_{10} of ~62 s (for 0.5% H_2) and 679 s (for 0.05% H_2), respectively. t_{10} is defined as the time taken for the sensor to recover to 10% of its baseline current from the peak value. Varying the body biases does not change the rate of the desorption reaction but has a dramatic effect on sensor t_{10}, with larger reverse biases enabling shorter t_{10}. This is primarily due to the different $I-V$ characteristics demonstrated by different reverse biases leading to varied current *vs* concentration relationships (see Supporting Information S4). Additionally, t_{10} can be further reduced by using integrated microheaters, which we have demonstrated in the past.[31] It is important to note that silicon CS-FETs will have a temperature dependence, requiring appropriate compensation for harsh environment operation. Results pertaining to this will be described in a future work. In all of the above measurements, the total power consumption of the hydrogen sensors is below 50 μW, reaffirming bulk silicon CS-FETs as a low-power gas-sensing platform.

Figure 4 compares the experimental data to simulation results, where simulated sensor responses are obtained at

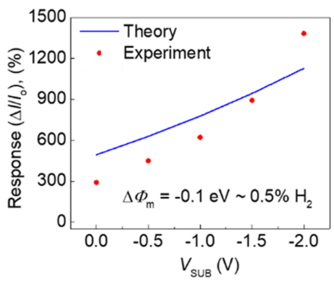

Figure 4. Theory *vs* experiment comparing sensor response. In experiment: V_{DS} = 3 V, RH < 10%, for theory sensing layer work function Φ_m = 4.2 eV.

different body biases for a constant −0.1 eV work-function change in the sensing layer (analogous to a simulated gas exposure of 0.5% H_2). As shown, the trend of increasing sensor responses with higher reverse body bias is consistent in both theory and experiment. However, the simulated work-function change does not capture the interaction between hydrogen and the sensing layer, which may explain the discrepancy in the trends.

Sensor Hysteresis, Ambient Drift, and Long-Term Stability. Several experiments were performed to gauge sensor hysteresis and long-term stability. Exposing the sensor to cycles of low (0.05%), medium (0.25%), and high concentrations (0.5%) of hydrogen indicates minimal hysteresis in sensor performance, as indicated by Figure 5a. Figure 5b captures the baseline drift of two sensors (V_{DS} = 3 V, V_{SUB} = 0 V) over a period of 5.7 days, where the sensors were measured in ambient air without any gas flow and uncontrolled room humidity. The maximum variation from mean baseline current in both sensors is approximately 10%, indicating stable sensor baselines. Additionally, bare silicon CS-FETs without any sensing layers also exhibit similar stability as depicted in Supporting Information S5. Figure 5c shows the variation in peak sensor response current to a fixed hydrogen concentration for nearly a week, where a sensor is exposed to 0.5% H_2 (for 10 min) once per day. This measurement was done at room temperature with the relative humidity left uncontrolled and varying between 20% and 40%. Based on these results, the CS-FET platform exhibits minimal sensor performance degradation and long-term stability. With respect to sensor selectivity, we previously demonstrated the Ni–Pd sensing layer to be selective to H_2S (hydrogen sulfide) and NO_2 (nitrogen dioxide) *via* multiplexed gas-sensing gas experiments. Detailed selectivity results of the bulk silicon CS-FETs in contextually defined applications will be described in a future work.

Benchmark Comparison with Emerging Low-Dimensional Materials. Finally, the performance of bulk silicon CS-FETs was benchmarked against emerging materials such as carbon nanotubes, MoS_2, and graphene for hydrogen gas sensing at the same concentration level (0.5%). Sensitive and fast detection at this concentration is important from a safety perspective, as it is below the lower explosion limit of 4%. This benchmark cites research works that have used both functionalized and nonfunctionalized materials. As indicated in Figure 6, bulk silicon outperforms these low-dimensional materials in terms of normalized sensor response (%). The results suggest that electrostatic charge confinement can be an effective route toward achieving high sensitivity with potential advantages over structural charge confinement.

CONCLUSION

To summarize, we have demonstrated chemical-sensitive field-effect transistors on bulk silicon, with an electrically floating ultrathin $Ni_{0.3\ nm}Pd_{1\ nm}$ sensing layer for H_2 gas sensing. Through device modeling and simulations, we have shown that by applying different V_{SUB} the sensitivity of the CS-FET can be tuned electrically. We have corroborated this by measuring the H_2 sensor response of fabricated Ni–Pd CS-FETs, which results in improved sensor linearity and recovery times. Moreover, this platform exhibits minimal sensor hysteresis and long-term drift. The results presented in this work build a compelling case for bulk silicon CS-FETs from both performance and manufacturability perspectives. This platform provides opportunities in a wide variety of applications such as industrial safety, environmental air quality monitoring, wireless sensor networks, and consumer electronics.

METHODS

CS-FET Device Modeling and Simulation. CS-FET device simulations in Figure 2 and Figure 4 were carried using Synopsys TCAD (Version M-2016.12). Carrier transport in devices is handled by self-consistently solving Poisson's continuity equation with the drift-diffusion model. The Philips unified model is used for calculating mobility in the devices. Quantum confinement effects associated with nanoscale devices are taken into consideration using the density-gradient-based quantization model. The Slotboom and Graaff band-

DOI: 10.1021/acsnano.8b00580
ACS Nano XXXX, XXX, XXX−XXX

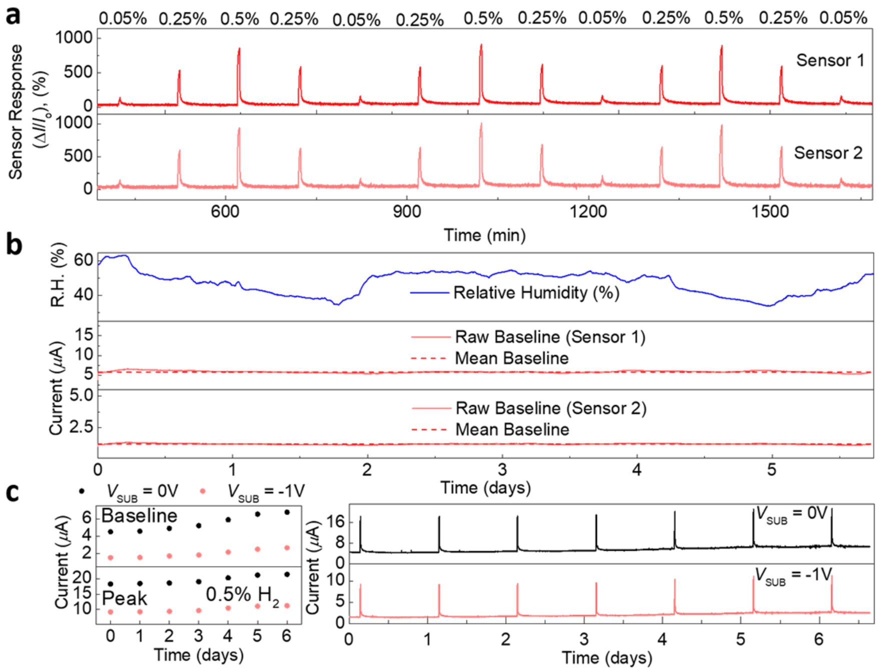

Figure 5. (a) H_2 concentration cycling for gauging sensor hysteresis of two Ni–Pd CS-FET sensors (V_{DS} = 3 V, V_{SUB} = −1.5 V, RH < 10%). (b) Still ambient drift characteristics of two Ni–Pd CS-FETs with uncontrolled relative humidity (V_{DS} = 3 V, V_{SUB} = 0 V). (c) Sensor baseline current, peak current, and response characteristics to multiple H_2 exposure pulses of 0.5% over 6 days (V_{DS} = 3 V).

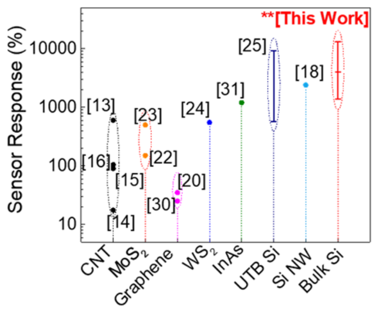

Figure 6. Performance benchmark at 0.5% H_2 concentration comparing different H_2 sensors reported in the literature based on emerging nanomaterials and bulk silicon (this work).

gap narrowing model is incorporated throughout the device. In addition to this, the doping-dependent Shockley–Reed–Hall recombination model is utilized in conjunction with the Hurkx band–band tunneling model.

CS-FET Fabrication Process. CS-FET gas sensors were fabricated on prime grade silicon ⟨100⟩ wafers with sheet resistivity in the range of 10–20 ohm·cm. A schematic representing the fabrication process is depicted in Supporting Information S1. Before processing, all wafers were cleaned in a standard piranha (1:4, hydrogen peroxide/sulfuric acid) bath at 120 °C and native oxide was removed using a 10 s dip in 1:10 hydrofluoric acid. First, a 350 nm silicon dioxide was thermally grown on the silicon wafers for device isolation, using a three-step dry (5 min)–wet (55 min)–dry (5 min) oxidation process at 1000 °C, at atmospheric pressure for 55 min. Oxide thickness was verified using fixed angle (70°) ellipsometry. Next, source and drain doping regions in silicon were defined using a standard i-line photolithography process (Fujifilm, photoresist: OiR 906-12, developer: OPD-4262) and wet etching the isolation oxide (in 5:1 buffered hydrofluoric acid for 5 min). Following this, an approximately 300 nm thick phosphosilicate glass (PSG) layer was deposited at 450 °C using low-pressure chemical vapor deposition (LPCVD). To complete the formation of n^{+2} doped regions, phosphorus drive-in and activation was performed in the silicon source and drain by rapid thermal annealing (RTA) at 1050 °C for 30 s in N_2. The PSG layer was then removed in a 1:10 hydrofluoric acid bath for 1 min. This process step involves overetching that can lead to some loss in field oxide from the original 350 nm, but is inconsequential to the overall device isolation. The "gate" or sensing layer region was patterned next and etched in 5:1 buffered hydrofluoric acid for 4 min. To define source and drain contacts, a separate source–-drain metallization mask was used, which underlaps the doped source and drain regions by 11 μm. After this, 50 nm of nickel was then deposited in the source and drain contact regions, using thermal evaporation and lift-off in acetone. To achieve ohmic source and drain contacts, nickel silicidation (NiSi) was performed in forming gas using an RTA at 420 °C for 5 min. Following this, an ultrathin Ni–Pd sensing layer was deposited by sequentially evaporating 1 nm Pd (using e-beam) and then 0.3 nm Ni (using thermal), without any vacuum break. Finally, the sensing layer was annealed in N_2 at 150 °C for 1 h postdeposition, which completed the sensor fabrication process.

Sensor Measurement Apparatus. All gas-sensing experiments described in this paper were done in a walk-in fume hood. CS-FET device chips were wire bonded to a 28-pin J-bend leaded chip carrier. A small-volume (∼0.83 cm^{-3}) 3D printed housing (made of polyactic acid) consisting of a 1/4 in. gas inlet was used to cover the chip carrier. Pure dry air was used as diluent gas and was procured from Praxair Technology Inc. For H_2 sensing experiments, 5% H_2 in N_2 (Praxair) was used as source. Ultra-high-purity H_2 (Praxair) was used for the experiment in Supporting Information S2. House-compressed dry air was used for week-long extended measurements (in Figure 5c). Typical gas flow rates were from 1 to 100 sccm, and diluent (air) flow rate was approximately 1000 sccm. Ambient temperature and humidity were monitored by commercial sensors purchased from Sensirion AG (models SHT2x and SHT3x). Gas delivery was controlled by mass flow controllers (Alicat Scientific Inc.). CS-FET sensors were biased using a Keithley 428 current preamplifier, and the current signals were acquired using a LabVIEW-controlled data acquisition unit (National Instruments, NI USB-6259). A Keysight 4155C semiconductor parameter analyzer was used for extended length ambient drift measurements in Figure 5b. Measurements in Supporting Information S4 were carried out using a different electronic readout setup and data acquisition board (National Instruments, NI-USB 6218).

DOI: 10.1021/acsnano.8b00580
ACS Nano XXXX, XXX, XXX−XXX

ASSOCIATED CONTENT

Supporting Information

The Supporting Information is available free of charge on the ACS Publications website at DOI: 10.1021/acsnano.8b00580.

> Bulk CS-FET fabrication process; H_2 sensor response characteristics of bulk CS-FETs with forming gas annealed Ni–Pd sensing layer; H_2 sensor response characteristics of bare (unfunctionalized) bulk CS-FETs; analysis of H_2 surface concentration, desorption rates, and correlation to sensor recovery at different V_{SUB}; ambient drift characteristics of bare (unfunctionalized) bulk CS-FETs; references (PDF)

AUTHOR INFORMATION

Corresponding Author

*E-mail (A. Javey): ajavey@berkeley.edu.

ORCID

Hossain M. Fahad: 0000-0002-6758-5432

Ali Javey: 0000-0001-7214-7931

Author Contributions

⊥H. M. Fahad and N. Gupta contributed equally to this work.

Author Contributions

H.M.F. and N.G. contributed equally to this work. H.M.F. led the project and fabricated the CS-FET sensors as well as device modeling and simulation. N.G. and H.M.F. carried out the measurements and analysis. N.G. and R.H. contributed to measurement setup and programming. S.B.D. contributed to device analysis. A.J. supervised the project. All authors discussed the results and wrote the paper.

Notes

The authors declare the following competing financial interest(s): H.M.F. and A.J. declare competing financial interests in equity on shares of Serinus Labs, Inc.

ACKNOWLEDGMENTS

A.J. acknowledges the Bakar Fellows Program in funding this research work. H.M.F. and N.G. thank H. Kim, D.-H. Lien, A.B. Sachid, and M. Amani for fruitful discussions.

REFERENCES

(1) Sun, Y.-F.; Liu, S.-B.; Meng, F.-L.; Liu, J.-Y.; Jin, Z.; Kong, L.-T.; Liu, J.-J. Metal Oxide Nanostructures and Their Gas Sensing Properties: A Review. *Sensors* **2012**, *12*, 2610–2631.

(2) Ponzoni, A.; Comini, E.; Sberveglieri, G.; Zhou, J.; Deng, S. Z.; Xu, N. S.; Ding, Y.; Wang, Z. L. Ultrasensitive and Highly Selective Gas Sensors Using Three-Dimensional Tungsten Oxide Nanowire Networks. *Appl. Phys. Lett.* **2006**, *88*, 203101–1.

(3) Favier, F.; Walter, E. C.; Zach, M. P.; Benter, T.; Penner, R. M. Hydrogen Sensors and Switches from Electrodeposited Palladium Mesowire Arrays. *Science* **2001**, *293*, 2227–2231.

(4) Li, X.; Liu, Y.; Hemminger, J. C.; Penner, R. M. Catalytically Activated Palladium@Platinum Nanowires for Accelerated Hydrogen Gas Sensing. *ACS Nano* **2015**, *9*, 3215–3225.

(5) Lundstrom, I.; Shivaraman, S.; Svensson, C.; Lundkvist, L. A Hydrogen-Sensitive MOS Field-Effect Transistor. *Appl. Phys. Lett.* **1975**, *26*, 55–57.

(6) Domansky, K.; Baldwin, D. L.; Grate, J. W.; Hall, T. B.; Li, J.; Josowicz, M.; Janata, J. Development and Calibration of Field-Effect Transistor-Based Sensor Array for Measurement of Hydrogen and Ammonia Gas Mixtures in Humid Air. *Anal. Chem.* **1998**, *70*, 473–481.

(7) Fukuda, H.; Seo, H.; Kasama, K.; Endoh, T.; Nomura, S. Highly Sensitive MOSFET Gas Sensors with Porous Platinum Gate Electrode. *Jpn. J. Appl. Phys.* **1998**, *37*, 1100–1102.

(8) Chakraborty, S.; Nemoto, K.; Hara, K.; Lai, P. T. Moisture Sensitive Field Effect Transistors Using $SiO_2/Si_3N_4/Al_2O_3$ Gate Structure. *Smart Mater. Struct.* **1999**, *8*, 274–277.

(9) Janata, J. Thirty Years of CHEMFETs – A Personal View. *Electroanalysis* **2004**, *16*, 1831–1835.

(10) Kong, J.; Franklin, N. R.; Zhou, C.; Chapline, M. G.; Peng, S.; Cho, K.; Dai, H. Nanotube Molecular Wires as Chemical Sensors. *Science* **2000**, *287*, 622–625.

(11) Qi, P.; Vermesh, O.; Grecu, M.; Javey, A.; Wang, Q.; Dai, H. Towards Large Arrays of Multiplex Functionalized Carbon Nanotube Sensors for Highly Sensitive and Selective Molecular Detection. *Nano Lett.* **2003**, *3*, 347–351.

(12) Khalap, V. R.; Sheps, T.; Kane, A. A.; Collins, P. G. Hydrogen Sensing and Sensitivity of Palladium-Decorated Single-Walled Carbon Nanotubes with Defects. *Nano Lett.* **2010**, *10*, 896–901.

(13) Mubeen, S.; Zhang, T.; Yoo, B.; Deshusses, M. A.; Myung, N. V. Palladium Nanoparticles Decorated Single-Walled Carbon Nanotube Hydrogen Sensor. *J. Phys. Chem. C* **2007**, *111*, 6321–6327.

(14) Suehiro, J.; Yamane, S.; Imasaka, K. Carbon Nanotube-Based Hydrogen Gas Sensor Electrochemically Functionalized with Palladium. *2007 IEEE Sensors*, Atlanta, GA, 2007; pp 554–557.

(15) Sun, Y.; Wang, H. H. High-Performance, Flexible Hydrogen Sensors that use Carbon Nanotubes Decorated with Palladium Nanoparticles. *Adv. Mater.* **2007**, *19*, 2818–2823.

(16) Li, X.; Thai, M. L.; Dutta, R. K.; Qiao, S.; Chandran, G. T.; Penner, R. M. Sub-6 nm Palladium Nanoparticles for Faster, More Sensitive H_2 Detection using Carbon Nanotube Ropes. *ACS Sens.* **2017**, *2*, 282–289.

(17) Han, J.-W.; Rim, T.; Baek, C.-K.; Meyyappan, M. Chemical Gated Field Effect Transistor by Hybrid Integration of One-Dimensional Silicon Nanowire and Two-Dimensional Tin Oxide Thin Film for Low Power Gas Sensor. *ACS Appl. Mater. Interfaces* **2015**, *38*, 21263–21269.

(18) Ahn, J.-H.; Yun, J.; Choi, Y.-K.; Park, I. Palladium Nanoparticle Decorated Silicon Nanowire Field-Effect Transistor with Side-Gates for Hydrogen Gas Detection. *Appl. Phys. Lett.* **2014**, *104*, 013508-1–013508-5.

(19) Schedin, F.; Geim, A. K.; Morozov, S. V.; Hill, E. W.; Blake, P.; Katsnelson, M. I.; Novoselov, K. S. Detection of Individual Gas Molecules Adsorbed on Graphene. *Nat. Mater.* **2007**, *6*, 652–655.

(20) Lange, U.; Hirsch, T.; Mirsky, V. M.; Wolfbeis, O. S. Hydrogen Sensor Based on a Graphene – Palladium Nanocomposite. *Electrochim. Acta* **2011**, *56*, 3707–3712.

(21) Hong, J.; Lee, S.; Seo, J.; Pyo, S.; Kim, J.; Lee, T. A Highly Sensitive Hydrogen Sensor with Gas Selectivity using a PMMA Membrane-Coated Pd Nanoparticle/Single-Layer Graphene Hybrid. *ACS Appl. Mater. Interfaces* **2015**, *7*, 3554–61.

(22) Kuru, C.; Choi, C.; Kargar, A.; Choi, D.; Kim, Y. J.; Liu, C. H.; Yavuz, S.; Jin, S. MoS_2 Nanosheet-Pd Nanoparticle Composite for Highly Sensitive Room Temperature Detection of Hydrogen. *Adv. Sci.* **2015**, *2*, 1500004–1.

(23) Hao, L.; Liu, Y.; Du, Y.; Chen, Z.; Han, Z.; Xu, Z.; Zhu, J. Highly Enhanced H_2 Sensing Performance of Few-Layer $MoS_2/SiO_2/Si$ Heterojunctions by Surface Decoration of Pd Nanoparticles. *Nanoscale Res. Lett.* **2017**, *12*, 567–1.

(24) Kuru, C.; Choi, D.; Kargar, A.; Liu, C. H.; Yavuz, S.; Choi, C.; Jin, S.; Bandaru, P. R. High-Performance Flexible Hydrogen Sensor made of WS_2 Nanosheet-Pd Nanoparticle Composite Film. *Nanotechnology* **2016**, *27*, 195501–1.

(25) Fahad, H. M.; Shiraki, H.; Amani, M.; Zhang, C.; Hebbar, V. S.; Gao, W.; Ota, H.; Hettick, M.; Kiriya, D.; Chen, Y.-Z.; Chueh, Y.-L.; Javey, A. Room Temperature Multiplexed Gas Sensing using Chemical Sensitive 3.5-nm-Thin Silicon Transistors. *Sci. Adv.* **2017**, *3*, e1602557.

(26) Penner, R. M. A Nose for Hydrogen Gas: Fast, Sensitive H_2 Sensors using Electrodeposited Nanomaterials. *Acc. Chem. Res.* **2017**, *50*, 1902–1910.

DOI: 10.1021/acsnano.8b00580
ACS Nano XXXX, XXX, XXX–XXX

(27) Conrad, H.; Ertl, G.; Latta, E. E. Adsorption of Hydrogen on Palladium Single Crystal Surfaces. *Surf. Sci.* **1974**, *41*, 435−446.
(28) Zhang, Y.; Pluchery, O.; Caillard, L.; Lamic-Humblot, A.-F.; Casale, S.; Chabal, Y. J.; Salmeron, M. Sensing the Charge State of Single Gold Nanoparticles *via* Work Function Measurements. *Nano Lett.* **2015**, *15*, 51−55.
(29) Neamen, D. A. *An Introduction to Semiconductor Devices*; McGraw-Hill: Boston, MA, 2006; pp 287−288.
(30) Phan, D.-T.; Chung, G.-S. Effects of Palladium Nanocrystal Morphologies on Hydrogen Sensors based on Palladium-Graphene Hybrid. *2015 IEEE Sensors*, Busan, South Korea, 2015; pp 1−4.
(31) Nah, J.; Kumar, S. B.; Fang, H.; Chen, Y.-Z.; Plis, E.; Chueh, Y.-L.; Krishna, S.; Guo, J.; Javey, A. Quantum Size Effects on the Chemical Sensing Performance of Two-Dimensional Semiconductors. *J. Phys. Chem. C* **2012**, *116*, 9750−9754.

DOI: 10.1021/acsnano.8b00580
ACS Nano XXXX, XXX, XXX−XXX